

Effective Suppression of Random-Dopant-Induced Characteristic Fluctuation Using Dual Material Gate Technique for 16 nm MOSFET Devices

Kuo-Fu Lee¹, Yiming Li^{1,2,*}, Chun-Yen Yiu¹, and Thet-Thet Khaing¹

¹Department of Electrical Engineering and Institute of Communications Engineering, National Chiao Tung University, Hsinchu 300, Taiwan

²National Nano Device Laboratories, Hsinchu 300, Taiwan

*Corresponding author. TEL: +886-3-5712121 ext: 52974; FAX: +886-3-5726639; and Email: ymli@faculty.nctu.edu.tw

1. Introduction

Threshold voltage (V_{th}) fluctuation has become a crucial problem for nowadays nano-CMOS devices. The random dopant fluctuation (RDF) has shown as the major source of variation [1-3]. Suppression of RD-induced V_{th} fluctuation is urgent for variability of sub-22-nm device technologies. Dual material gate (DMG) was recently proposed to improve device performance [4]. However, RDF of DMG devices is not reported yet. In this work, we for the first time explore the DMG and inverse DMG devices for suppressing RDF-induced characteristics fluctuation in 16-nm MOSFET devices. The physical mechanism of DMG devices to suppress RDF are investigated and discussed. The results of this study show that device with DMG possesses fascinating reduction of RDF-induced fluctuations.

2. Simulation Configuration and Results Discussion

The control device prepared in this work is with TiN/HfSiON gate stack of 0.8-nm EOT. The gate length and width are 16 nm and the work function is 4.52 eV. The V_{th} is calibrated to 250 mV for all devices according to ITRS roadmap for low-operating-power application. The statistically random generated discrete dopants are incorporated into the large-scale three-dimensional (3D) device simulation, which has been developed by us recently [1], as shown in Figs. 1(a)-(c). In which 1327 dopants are randomly generated in a large cube. Then, the large cube is partitioned into 216 3D sub-cubes and mapped into device channel region. The quantum mechanically corrected transport simulation is performed by solving a set of 3D density-gradient equation coupling with drift-diffusion equations. The characteristic fluctuation of devices was validated with respect to experimentally measured data to ensure the best accuracy [5]. Second, device with dual material gate has two types, DMG and inverse DMG, as shown in Fig. 1(d). For DMG device, the work function (WK) at the source and drain sides are WK1 and WK2, respectively, and WK1 > WK2. The inverse DMG device are designed accordingly, and WK1 < WK2. The gate materials could be MoN, TiN, and Ta, whose distributions of grain orientation and work-function are summarized in Fig. 1(e) [4].

For the higher WK near the source side or the drain side, it may induce higher intrinsic electrostatic potential barrier for both on- and off-state, as shown in Fig. 1(f). The RDs induce rather different potential profiles due to WK difference in spite of the same number and position of dopants, as disclosed in Figs. 2(a)-(c). Therefore, the I_D - V_G fluctuations induced by RDs for inverse DMG and DMG devices are further presented in Figs. 2(d)-(e), respectively. The inset tables of Figs. 2(d) and 2(e) list their nominal value and normalized variations (the standard deviation divided by the mean value of DC characteristics). The DMG device shows smaller DC characteristic fluctuations, the V_{th} fluctuations are 51.9 mV and 30.8 mV for inverse DMG and DMG devices, respectively. The normalized I_{on} and I_{off} variations of DMG device are 14% and 80%, and they are smaller than those of inverse DMG device, 18% and 87%. To examine the physical insights, the same dopants number and position induced potential energies are shown in Fig. 3. The dopants will induce potential deviation Φ_{dopant} , and the high, low, and control WK-induced potential barriers are Φ_H , Φ_L , and Φ_M , respectively, as shown in Fig. 3. In Figs. 3(a)-(d), the dopant will induce relatively smaller potential deviation in DMG due to a

larger initial potential barrier existed (Φ_{dopant}/Φ_H , compared with Φ_{dopant}/Φ_L and Φ_{dopant}/Φ_M) in the cross-sectional view of potential energies for dopant near the source side. Therefore, the DC characteristic fluctuations in DMG are dramatically reduced. However, the same phenomenon for dopant near the drain side can not enjoy the advantage in the inverse DMG structure because the carrier controllability is totally decided at the source edge, as shown in Fig. 3(e)-(h). The comparison of I_D - V_G , potential, electron velocity, and lateral electric field for DMG and control devices are further examined, as shown in Fig. 4. For Fig. 4(a), the DMG device shows an abrupt potential step in the middle of the channel. This abrupt potential step mainly comes from the WK difference of different gate materials and this potential profile of the DMG device results in locally enhanced lateral electric field inside the channel. For Fig. 4(b), the control device attains its maximal electric field peak near the drain according to a classical electric field profile. However, the studied DMG device has electric field peak inside the channel as well as near the drain. Locally generated electric field inside the channel results in a relatively higher carrier velocity, where Fig. 4(c) shows velocity profiles along the channel direction. Therefore, DMG device has larger I_{on} in the similar I_{off} compared with the control device, as shown in Fig. 4(d). The trend of the dopant number and position effect in DC characteristics of DMG and control device could be confirmed according to our recent work [5], as display in Figs. 4(e)-(h). For the dopant number increases as equivalent channel doping concentration increases, this substantially alters the V_{th} , the I_{on} and I_{off} . Additionally, the position of RDs induces different fluctuations of characteristics in spite of the same number of dopants, as marked in inset of Fig. 4(h). Finally, as listed in Fig. 4(i), the table summarizes the suppression techniques for DMG, compared with our recent studies [6-8], the improvement of DMG for suppressing the RDF-induced V_{th} , I_{on} , and I_{off} fluctuation are 28%, 12.3%, and 59%, respectively, which is a enthralling method compared with other suppression techniques.

3. Conclusions

In this work, we have estimated DMG and inverse DMG techniques for suppressing RD-induced characteristics fluctuations for 16-nm MOSFET devices. The device with DMG exhibits the most effective way to reduce DC characteristic fluctuations, compared with the inverse DMG and control samples. We are currently conducting sample fabrication and measurement for this technique. Suppression of AC characteristic fluctuation is under investigation.

Acknowledgement

This work was supported in part by Taiwan National Science Council (NSC) under Contract NSC-97-2221-E-009-154-MY2 and by the TSMC, Taiwan, under a 2009-2010 grant. Mr. K.-F. Lee would like to thank Mr. M.-H. Han and Professor H. Watanabe for their stimulating discussion.

References

- [1] Y. Li *et al.*, IEEE T ED, vol. 57, (2010), pp. 437-447.
- [2] Y. Li *et al.*, IEEE T ED, vol. 56, (2009), pp. 1588-1597.
- [3] A. Asenov *et al.*, in *IEDM*, (2008), pp.1-1.
- [4] S. Chakraborty *et al.*, IEEE T ED, vol. 55, (2008), pp. 827-832.
- [5] Y. Li *et al.*, IEEE T ED, vol. 55, (2008), pp. 1449-1455.
- [6] K.-F. Lee *et al.*, Semicond. Sci. Tech., vol. 25, (2010), 045006.
- [7] Y. Li *et al.*, in IEEE SISPAD, (2008), pp. 22-1-22-4.
- [8] M.-H. Han *et al.*, Jpn. J. Appl. Phys., vol. 49, (2010), 04DC02.

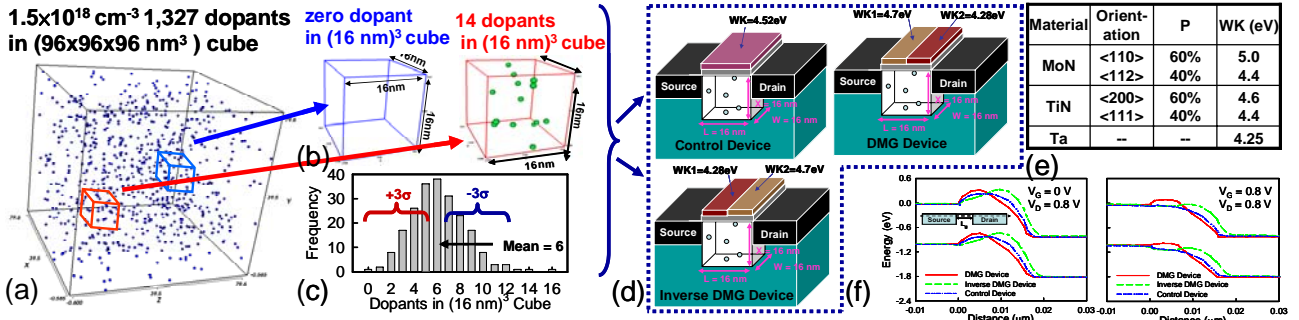


Fig. 1. (a) 1327 dopants are randomly generated in a large cube of $96 \times 96 \times 96 \text{ nm}^3$, in which the equivalent doping concentration is $1.5 \times 10^{18} \text{ cm}^{-3}$. The large cube is then partitioned into 216 sub-cubes of $16 \times 16 \times 16 \text{ nm}^3$. The number of dopants in sub-cube may vary from 0 to 14, and the average number is 6 ((b)-(c)). (d) These 216 sub-cubes are equivalently mapped into channel region of control, DMG, and inverse DMG devices. (e) The properties of metal material used in this work (f) The energy band diagram of off-state and on-state for control, DMG and inverse DMG nominal device, respectively.

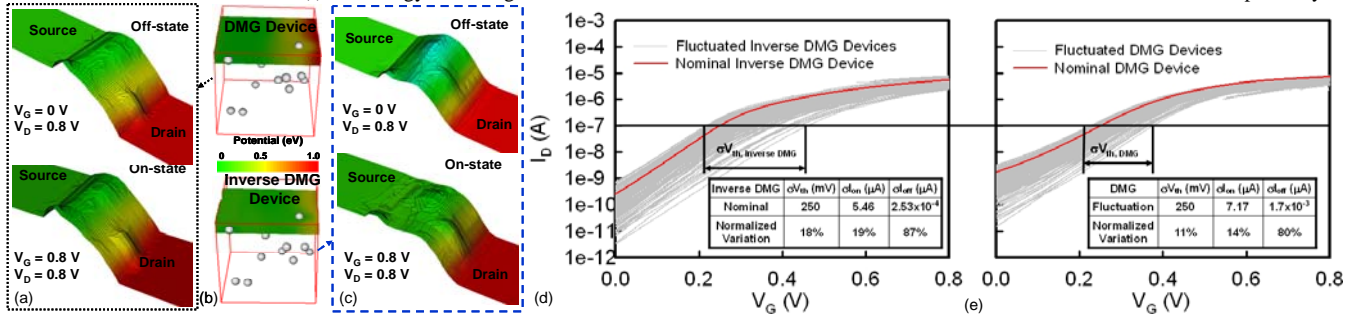


Fig. 2. The 14 random dopants induce difference in potential profiles which are extracted from (b) between the on-state and the off-state for (a) DMG and (c) inverse DMG device. The I_D - V_G curves of (d) inverse DMG and (e) DMG devices. The nominal values and normalized characteristic variations for inverse DMG and DMG devices are summarized in the insets, respectively.

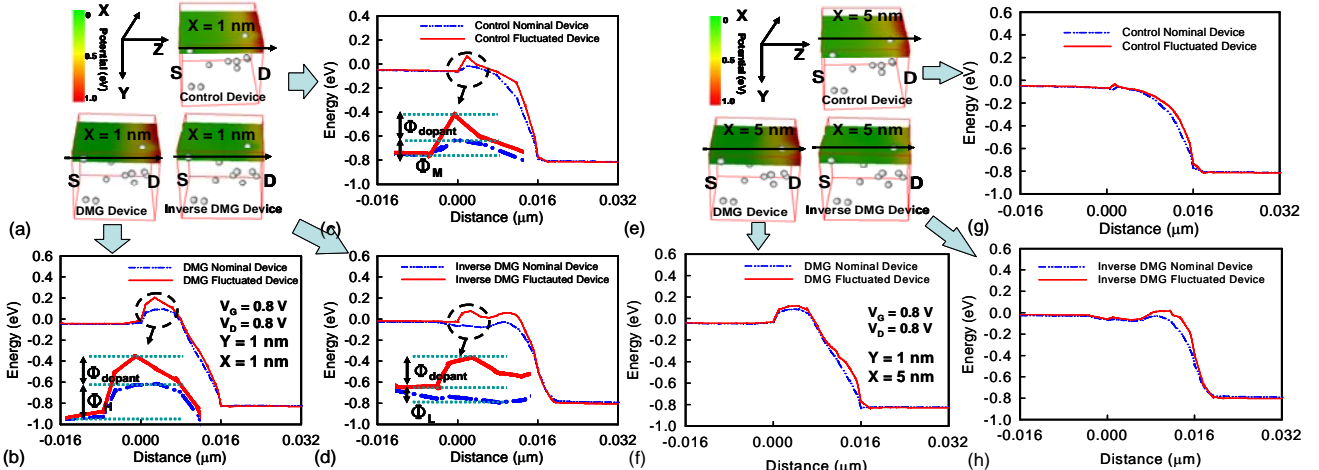


Fig. 3. (a) and (e) The surface potential energy induced by 14 random dopants for control, DMG and inverse DMG devices, respectively. (b)-(d) the slices of potential energy for dopant near the source side. (f)-(h) the slices of potential energy for dopant near the drain side.

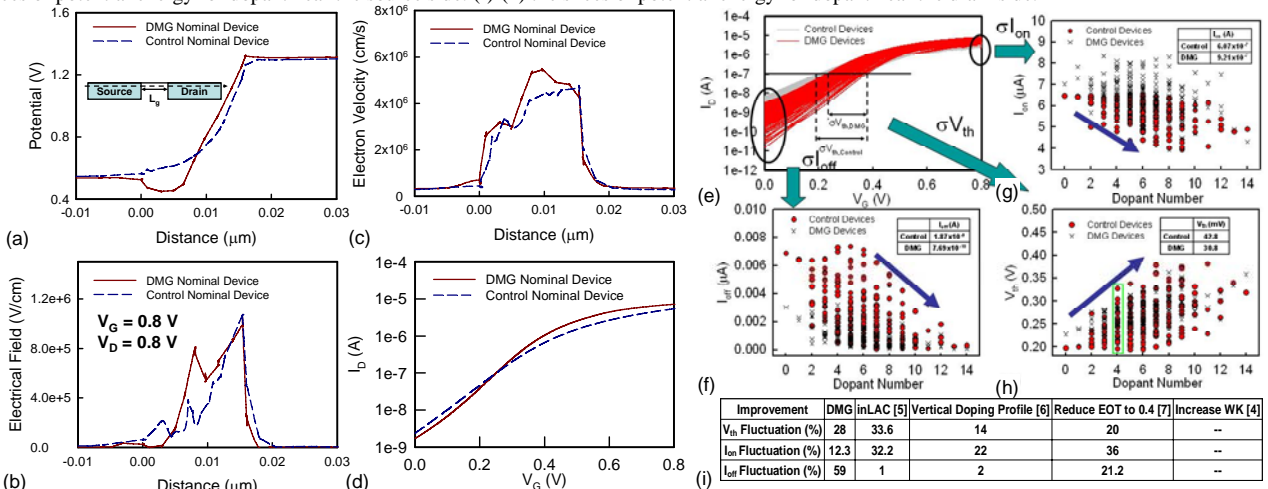


Fig. 4. Comparison of nominal (a) surface potential, (b) lateral electric field, (c) electron velocity, and (d) I_D - V_G curve for DMG device and control sample. (e) Comparison of RD-fluctuated I_D - V_G curves of DMG device (red line) and control sample (gray line). (f) I_{off} , (g) I_{on} , and (h) V_{th} fluctuations extracted from (e). (i) Summarization of DC characteristic fluctuations improvement in this work.